JOURNAL OF Materials CHEMISTRY

Aluminium oxide nanoparticles prepared by water-in-oil microemulsions

Yong-Xin Pang and Xujin Bao*

Institute of Polymer Technology and Materials Engineering, Loughborough University, Loughborough, Leicestershire, UK LE11 3TU. E-mail: x.bao@lboro.ac.uk

Received 4th July 2002, Accepted 10th September 2002
First published as an Advance Article on the web 15th October 2002

A new water-in-oil microemulsion, consisting of the non-ionic surfactant Triton X-114, cyclohexane as the oil phase and 1.0 M $AlCl_3$ aqueous solution as the aqueous phase, was developed and used to synthesise aluminium oxide (Al_2O_3) nanoparticles. The partial phase diagram of this ternary system was also determined at 38 °C. Syntheses of Al_2O_3 nanoparticles were carried out in a range of microemulsions with a fixed oil : surfactant ratio of 70 : 30 (w/w), but with different aqueous phase contents. For the purposes of comparison, Al_2O_3 particles were also synthesised in the corresponding emulsion and by direct precipitation from aqueous solution. Nano-sized Al_2O_3 particles were only obtained *via* microemulsions, whereas the emulsion route led to hollow ball-shaped particles with sub-micron apparent sizes and the direct precipitation process resulted in angular particles about 250 nm in dimension. The nanoparticles synthesised in the microemulsion with 20 wt% aqueous phase content have smaller particle sizes (5–15 nm) and a lower transformation temperature into α-form Al_2O_3 crystallites. Pure α-Al_2O_3 nanocrystals were obtained by calcination at 1000 °C for 12 h, while the nano-sized dimension of the particles retained though the apparent particle size increased to some extent. This transformation temperature is about 200 °C lower than that for the Al_2O_3 particles synthesised by direct precipitation.

1 Introduction

Microemulsions are optically transparent and isotropic, thermodynamically stable oil-in-water (O/W) or water-in-oil (W/O) dispersions stabilised with surfactant molecules.[1] The domain size of the dispersed phase in microemulsions is usually very small (a few nanometres) and chemical reactions may occur within the nanodroplets or at the oil–water interface in microemulsions.[2] Microemulsions can be made very stable with respect to the salinity of the aqueous phase, time and temperature by choosing suitable components and environmental conditions. These special physicochemical properties allow materials scientists to use microemulsions as media for the synthesis of new materials, especially nano-sized particulates.[3]

Syntheses of ultrafine ceramic particles *via* microemulsions has attracted a geat deal of attention in recent years. Arriagada and Osseo-Asare[4] synthesised nanosized silica by base-catalysed hydrolysis of tetraethoxysilane in a W/O microemulsion consisting of Triton X-100 (surfactant), cyclohexane and ammonia. The resulting silica particle sizes were around 30–70 nm. Wang *et al.*[5] reported the preparation of zirconia nanoparticles in a microemulsion with cyclohexane as the oil phase, NP-5 and NP-9 as the surfactants, and 0.75 M $ZrO(NO_3)_2$ aqueous solution as the aqueous phase. Ultrafine titania,[6] lead zirconate,[7] lead zirconate titanate[8] and hydroxyapatite[9] particles have been synthesised in similar microemulsions by using different salt solutions as aqueous phases. Microemulsion processing was also used to synthesise mixed ceramic nanoparticles such as zirconia–silica nanospherical particles,[10] binary metal oxides (TiO_2, ZrO_2) and ternary metal oxides ($BaTiO_3$, $BaZrO_3$).[11] More recently, Balint *et al.*[12] reported the synthesis of barium-stabilised alumina nanoparticles *via* a combination of microemulsion and hydrothermal routes. The microemulsion consisted of isooctane, polyethylene glycol, propanol and the aluminium and barium isopropoxides. They found that the barium oxide was essential for obtaining high surface area nanoparticles, but, in turn, it restricted the transformation of the precursor into α-form alumina. Tartaj and Tartaj[13] synthesised iron oxide-doped alumina nanoparticles through microemulsions comprising cyclohexane, Ipegal C-520 (surfactant) and the aqueous solution of the metal nitrates. The existence of iron oxide reduced the transformation temperature of the precursor into α-form alumina.

Aluminium oxide (Al_2O_3) is one of the most versatile ceramic oxides and has been used in a wide range of applications in electrical, engineering and biomedical areas, depending on its purity and crystallinity. Al_2O_3 is commercially produced from bauxite at low cost, but the purity and particle morphology are not suitable for many applications. Preparation of high purity fine alumina particles is of greater importance for advanced applications. Chemical precipitation from aqueous solutions of aluminium salts is a convenient and cost-effective method that has been widely used over the years.[14,15] The sol–gel route has also attracted a great deal of attention and has been intensively studied in recent years.[16–18] This process has the advantage of being able to be used for the formation of homogeneous films and, in some cases, can be used to produce α-form Al_2O_3 crystals at comparatively low temperatures. However, the starting materials, usually aluminium alkoxides, are relatively expensive. In addition, some other methods, such as microwave combustion,[19] arc plasma,[20] *etc.*, have also been used for alumina synthesis. In this research, a new microemulsion system has been developed to synthesise alumina nanoparticles. The aim of this study is to discuss the feasibility of the microemulsion route for the preparation of nano-sized alumina particles and to compare the particle dimensions and morphology, as well as the calcination behaviour, of the synthesised nanoparticles with those prepared by emulsion and direct precipitation routes.

2 Experimental

2.1 Materials

Aluminium chloride hexahydrate, ammonia (28% aqueous solution), Triton X-114, cyclohexane and ethanol (95%) were

all purchased from Fisher Scientific UK and were used as received. Distilled water was used throughout the experiments.

2.2 Phase diagram determination

The phase diagram of the ternary system consisting of cyclohexane, Triton X-114 and 1.0 M $AlCl_3$ aqueous solution was determined at 38 °C. The surfactant was first dissolved in cyclohexane in a cylinder flask fitted with a magnetic stirrer and a conductivity meter probe (HANNA Instruments, model HI 8633). Then, the flask was immersed in a water bath maintained at 38.0 ± 0.2 °C. After stirring for 30 min, the aqueous phase (1.0 M $AlCl_3$ aqueous solution) was dropped into the oil phase with continuous stirring. After addition of the first drop, the next drop of aqueous solution was not added until the system returned to a transparent state, and this procedure was continued for subsequent additions. Meanwhile, the conductivity of the system was recorded at intervals during the process. When the composition was close to the microemulsion–emulsion boundary, the system returned to a transparent state very slowly. The point at which the system did not return to a transparent state after 30 min was taken as the microemulsion–emulsion boundary. The transparency of the system was judged by visual observation.

2.3 Synthesis of Al_2O_3 nanoparticles

The syntheses of Al_2O_3 precursors were conducted in the water-in-oil microemulsions with a fixed cyclohexane : surfactant ratio of 70 : 30 (w/w) but with different aqueous phase contents, *i.e.* along the dash-dot line in the partial phase diagram (Fig. 1). The microemulsion compositions used for these syntheses are listed in Table 1. The microemulsions with different aqueous phase contents were first prepared as described in the previous section. The $AlCl_3$ in the aqueous phase of these microemulsions was hydrolysed by dropwise addition of ammonia solution to form the Al_2O_3 precursors. A slight excess of ammonia was required to set the reaction system pH at 9.5. The system was kept stirring at 38 °C for 24 h after addition of ammonia solution. Then, approximately a twofold volume of ethanol was added into the reaction system and stirring maintained for another 30 min. Afterwards, the mixture was centrifuged to reclaim the precipitated Al_2O_3 precursor. Five cycles of ethanol washing and centrifuging followed by three cycles of water washing and centrifuging were performed in order to remove surfactant residue and water soluble salts. The precipitates were dried in a vacuum oven at 70 °C for 24 h prior to calcination.

Calcination of the powder samples was carried out in a tube furnace and with a ramp rate of 2.0 °C min^{-1}. Samples were calcined to different temperatures for a fixed time or to a constant temperature for various durations.

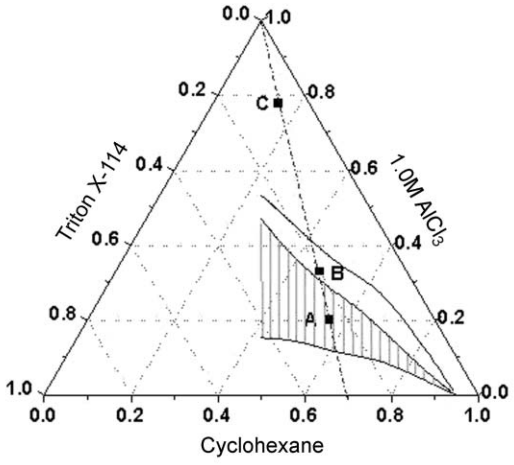

Fig. 1 Partial phase diagram of the cyclohexane, Triton X-114 and 1.0 M $AlCl_3$ ternary system at 38 °C.

Table 1 Microemulsion and emulsion compositions for syntheses of Al_2O_3 particles

	CH : X-114 : 1.0 M $AlCl_3$ mass ratio[a]	
Sample	Initial	After adding NH_3 (aq)
A	0.56 : 0.24 : 0.20	0.52 : 0.22 : 0.26
B	0.47 : 0.20 : 0.33	0.43 : 0.19 : 0.38
C	0.15 : 0.07 : 0.78	0.12 : 0.05 : 0.83
D	$AlCl_3$ (aq)	

[a]CH stands for cyclohexane.

2.4 Characterisation

The particle morphology of the as-prepared Al_2O_3 precursor and the calcined products was observed by transmission electron microscopy (TEM; JEOL JEM 100CX). TEM samples were prepared by dropping powder dispersions onto copper grids covered with carbon film.

The morphology of sintered samples was observed using a field emission gun scanning electron microscope (FEGSEM; LEO 1530 VP). Sample discs were prepared by uniaxial compaction at 500 MPa and then sintered at 1200 °C for 2 h. The sample surface was polished and etched before observation.

The phase compositions of the as-prepared and calcined products were analysed by X-ray diffraction (XRD) using a Bruker AXS D8 Advance diffractometer employing Cu-K_α radiation at 40 kv and 40 mA. Data were collected over the 2θ range of 20 to 70° at a step size of 0.02° and a step time of 0.5 s. In order to use the diffraction peak height as a semi-quantitative estimate of crystallinity, the sample loading was always 200 mg spread over a 3 × 3 cm area for all measurements. Special care was taken to keep the measurement conditions as identical as possible.

The crystallite sizes of the samples after calcination at 1200 °C for 2 h were estimated using Scherrer's formula:

$$X_s = 0.9\lambda/(\mathrm{FWHM}\cos\theta)$$

where X_s is the crystallite size in nm, λ is the wavelength (in nm) of the monochromatic X-ray beam (λ = 0.15406 nm for Cu-K_α radiation), FWHM is the full width at half maximum (in rad) for the diffraction peak under consideration (the inherent broadening of the equipment was ignored in the FWHM measurements) and θ is the diffraction angle in degrees.

3 Results and discussion

3.1 Microemulsion phase diagram analysis

The partial phase diagram determined for the ternary system of Triton X-114, cyclohexane and 1.0 M $AlCl_3$ aqueous solution is shown in Fig. 1. The heavy line marks the microemulsion–emulsion boundary. Under this curve, the system forms optically transparent water-in-oil (W/O) microemulsions. While above the curve, the system forms opaque W/O emulsions. It is well known that there are various internal microstructures in the transparent microemulsion region.[21,22] The shaded area within the microemulsion region shows the bicontinuous microstructure, which is relatively large in this phase diagram. Below the shaded area (the high oil content side), the aqueous phase is dispersed in the oil as micelles, and most of them are combined with the surfactant. These microemulsions with lower aqueous phase contents have relatively low viscosities. Above the bicontinuous region, the W/O microemulsions consist of surfactant film-coated water

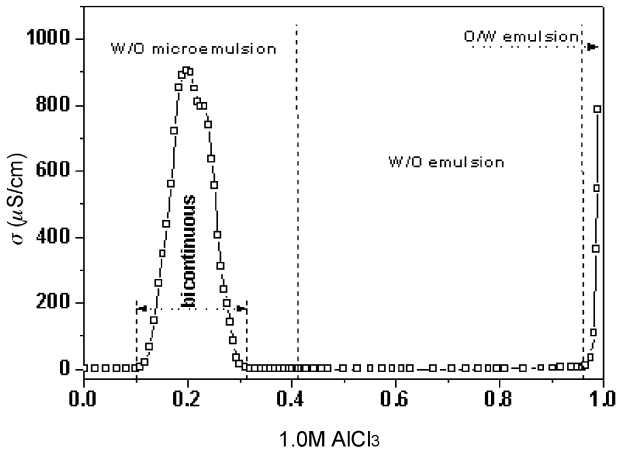

Fig. 2 Two-dimensional phase diagram for a fixed cyclohexane-to-surfactant ratio of 70 : 30 by mass.

droplets which are dispersed in the continuous oil phase.[2,21] The viscosities of these microemulsions are relatively high compared with those with lower water contents, though they all show very low conductivities.

Oil-in-water (O/W) emulsions may, however, exist at higher aqueous phase contents as a result of phase inversion. Although phase inversion from W/O to O/W emulsions is not the subject of this paper, we have determined the phase inversion for a system with an oil : surfactant ratio of 70 : 30 (w/w). It was found that the phase inversion took place at a very high aqueous phase content, 96.5 wt%, based on conductivity measurements. The conductivity of this system as a function of aqueous phase content is shown in Fig. 2. In the microemulsion region, the system is transparent. The high conductivity in this region indicates the bicontinuous microstructure of the microemulsion. In the W/O emulsion region, the system is opaque and the conductivity is very low. It should be noted, however, that the boundary between microemulsion and emulsion is not very sharp. There is always a translucent transient state encountered when the system changes from transparent (microemulsion) to opaque (emulsion). The vertical dashed line in Fig. 2, which shows the microemulsion–emulsion boundary, is drawn at the phase ratio where the system changes from transparent to translucent. It was also found that there was no obvious change in system appearance during the phase inversion from W/O to O/W emulsions. However, the significant decrease in viscosity and increase in conductivity of the system accompanying the phase inversion were clearly observed (Fig. 2).

The phase diagram at higher surfactant content (surfactant : oil $>$ 1 : 1 w/w) was not determined due to the very high viscosity of the system. Actually, if the surfactant content was greater than the amount of oil, the system became a gel at higher aqueous phase contents. This restricted the effective mixing of the aqueous phase with the oil phase, though the system was still in the microemulsion region.

3.2 Synthesis and characterisation of Al_2O_3 nanoparticles

Syntheses of Al_2O_3 precursors were carried out in the W/O microemulsions and emulsion by hydrolysis of the aluminium chloride in the aqueous phase with ammonia solution. Here, the nanodroplets in a W/O microemulsion are used as nanoreactors and the microdroplets in the W/O emulsion as microreactors. Nanoparticles are usually obtained if chemical reaction-induced precipitation takes place within the nanopools of salt solution in the microemulsion and the coalescence of formed particles is, to some extent, constrained by the surfactant film coating the nanopools. In this study, W/O microemulsions and an emulsion with a fixed cyclohexane : surfactant ratio of 70 : 30 (w/w), but with various aqueous phase contents, designated A, B and C in Fig. 1, were chosen for the syntheses. These microemulsions have different microstructures, as shown in Fig. 1. It is worthwhile checking whether the microemulsion microstructures have any effects on the morphology and properties of the synthesised inorganic particles.

Fig. 3 shows TEM micrographs of the Al_2O_3 particles synthesised in the compositions A–C; Fig. 3(a)–(c) correspond to samples A–C. Sample A consists of highly agglomerated nanoparticles, with the mean particle size being about 8 nm. The nanoparticles are somewhat elongated and the length-to-width aspect ratio is about 2. Sample B shows particle sizes and

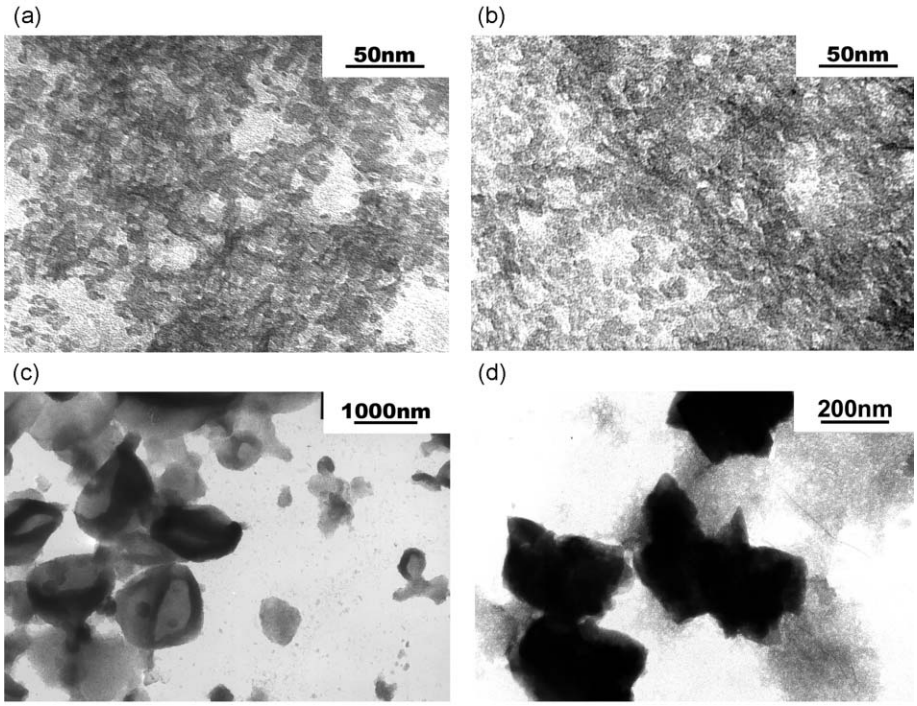

Fig. 3 TEM micrographs of the as-synthesised Al_2O_3 precursors. (a)–(d) Correspond to samples A–D, respectively.

morphology similar to sample A, but the aspect ratio is lower and the nanoparticles are slightly more spherical compared with sample A. These results are consistent with the microstructure of the microemulsions. The aqueous phase is elongated to form a continuous network that penetrates through the continuous oil phase in the bicontinuous microemulsions. Sample A was synthesised in such a bicontinuous microemulsion, so the resulting nanoparticles show the elongated shape. Sample C contains spherical particles that look like hollow balls with parts of the walls having collapsed [Fig. 3(c)]. The particle size is about 1000 nm and the size distribution is wide. The large particle size results from the large dimensions of the dispersed phase in the W/O emulsion. Since the precipitation reaction is very fast, the diffusion of the precipitant (ammonia) into the water pools governs the formation of the precipitates. The hollow ball structure could be expected if the water pool size is large enough, because the precipitation reaction would have finished as soon as the precipitant penetrates through the surfactant film and contacts with the salt solution in the water pool. In addition, TEM observation at higher magnification revealed that the spherical shells were composed of nanoparticles, as shown in Fig. 4. This may be due to the complexation of aluminium cations with the ethylene oxide chains in the surfactant, which prevents the precipitates from growing to some extent. On the other hand, the hollow particles were not very mechanically strong and parts of their shells collapsed during washing and drying, resulting in the observed morphology. Thus it can be seen that the particle sizes and morphologies are quite different for the samples synthesised in the microemulsions and the emulsion. The nanoparticles can only be obtained in microemulsions.

For the purposes of comparison, sample D was prepared by direct precipitation from the corresponding aqueous solution under the same pH and temperature conditions. A TEM micrograph of this precipitate (sample D) is shown in Fig. 3(d). The particle size of sample D is about 250 nm and the morphology is more angular compared with those obtained from the microemulsions and the emulsion.

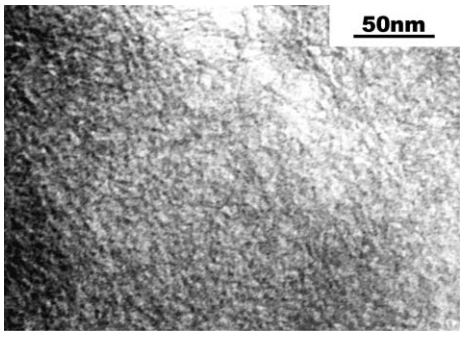

Fig. 4 TEM image of the microstructure of the spherical shells in sample C.

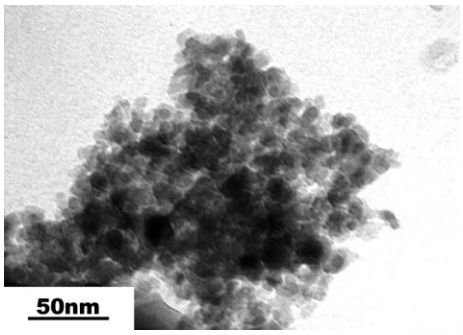

Fig. 5 TEM micrograph of sample A after calcination at 1000 °C for 12 h.

Fig. 5 shows a TEM micrograph of sample A after calcination at 1000 °C for 12 h. The nanoparticles are readily identifyable in the micrograph, although they are aggregated. Compared to the as-prepared nanoparticles, the particle dimensions increased and the size distribution became wider after calcination, as expected, due to coarsening during the calcination. Similar results were obtained for other samples. However, the nanoparticles were retained under such calcination conditions, with the mean size increasing to about 15 nm, as shown in Fig. 5. The XRD measurements (Fig. 10, discussed below) reveal that these nanoparticles are α-form Al_2O_3 crystals.

The morphology of compacts made from the precursor particles was also observed by FEGSEM. Fig. 6 shows that the grain sizes are still very small (about 200 nm) in these compacts after sintering at 1200 °C for 2 h. However, the compact made from sample A has slightly smaller and more uniform grain sizes compared with the others, while the compact of sample D displays the widest grain size distribution. These FEGSEM micrographs also indicate that the sample A compact has the lowest porosity among the three, suggesting good densification behaviour.

The XRD spectra of these four samples after calcination at different temperatures are shown in Fig. 7–9. The as-prepared particles are mainly amorphous, but the four broad peaks indicate the existence of boehmite.[23] Boehmite and bayerite are usually formed under alkaline conditions, as the amount of OH^- ions increaces with the addition of ammonia.[14]

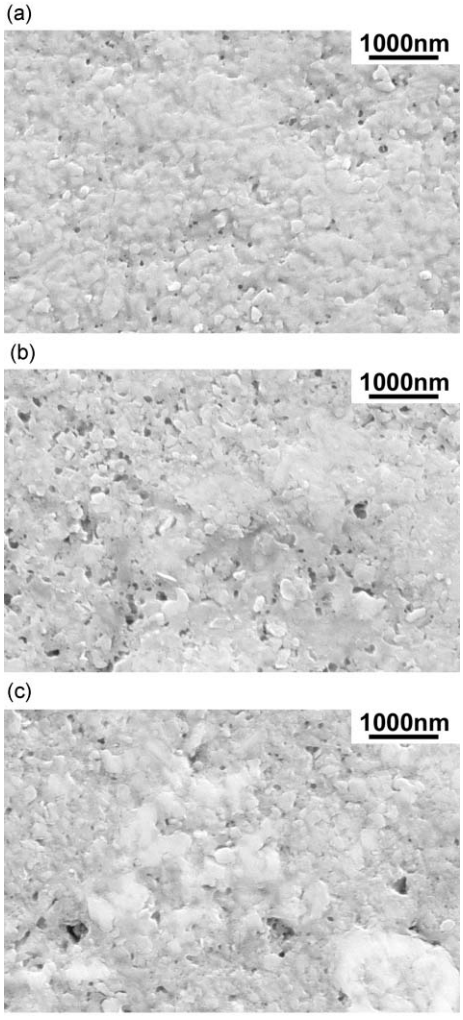

Fig. 6 FEGSEM micrographs for the compacts after sintering at 1200 °C for 2h. (a), (b) and (c) Correspond to compacts prepared from samples A, C and D, respectively.

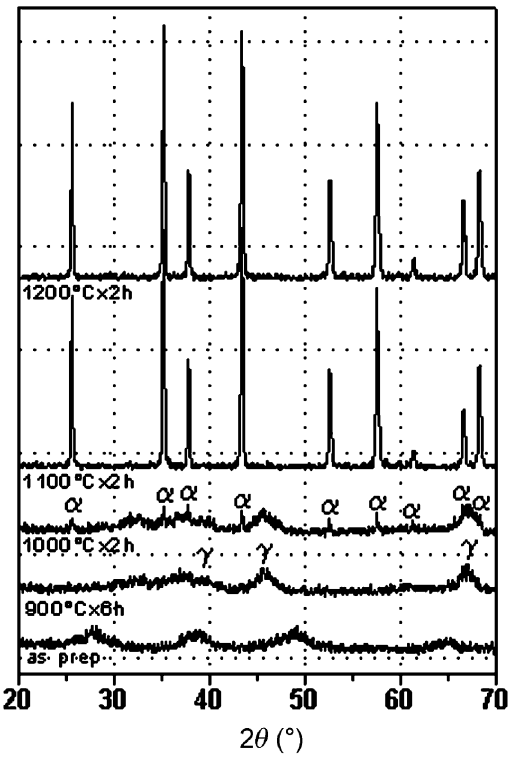

Fig. 7 XRD spectra for sample A synthesised in the bicontinuous microemulsion after calcination at various temperatures.

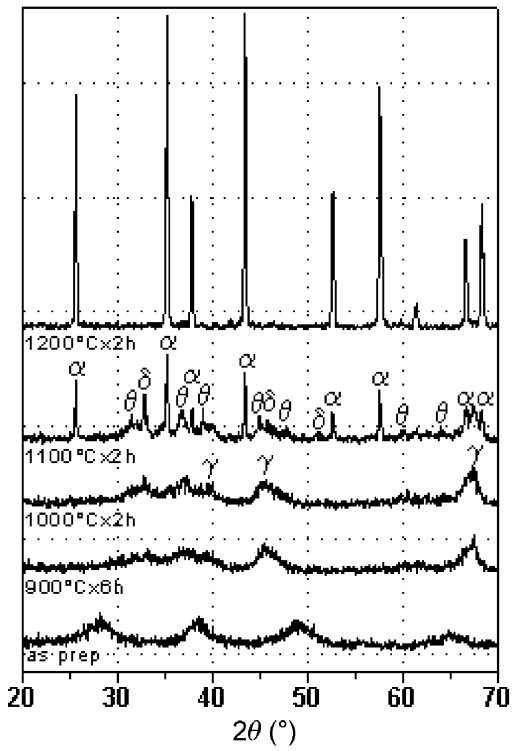

Fig. 8 XRD spectra for sample C synthesised in the emulsion after calcination at various temperatures.

Calcination at 900 °C for 6 h converts the materials into γ-form aluminium oxide (γ-Al_2O_3), but there are small amounts of θ- and δ-Al_2O_3 present in sample D, as shown in the corresponding XRD spectra (Fig. 9).[14] After calcination at 1000 °C for 2 h, α-Al_2O_3[14,16] and γ-Al_2O_3 are formed in sample A. Extending the calcination time leads to the transformation of γ-Al_2O_3 into pure α-Al_2O_3. This trend is clearly shown in

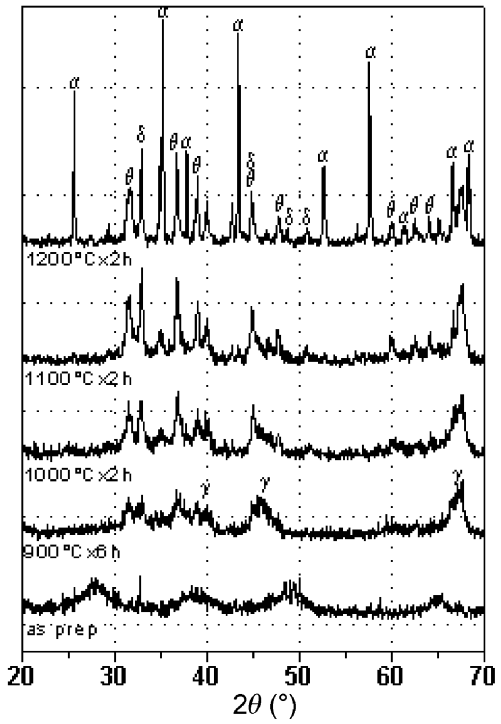

Fig. 9 XRD spectra for sample D synthesised by direct precipitation from aqueous solution after calcination at various temperatures.

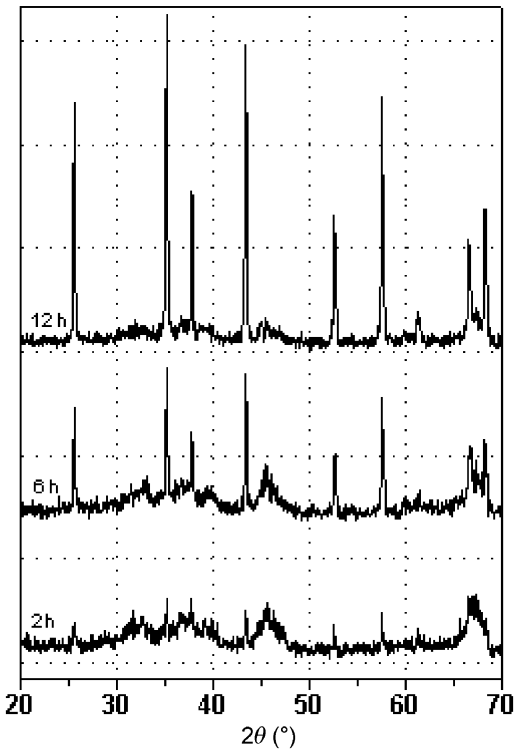

Fig. 10 Conversion of sample A precursor to α-Al_2O_3 at 1000 °C as a function of calcination time.

Fig. 10. On the other hand, sample C still remains as γ-Al_2O_3, with a very few θ-form crystals present, and sample D mainly in the θ- and δ-forms after calcination at 1000 °C for 2 h. After calcination at 1100 °C for 2 h, only α-Al_2O_3 diffraction peaks are observed for sample A, but diffraction peaks for α-Al_2O_3, as well as other Al_2O_3 crystalline forms, are clearly seen in the spectra of samples B and C. Surprisingly, no α-Al_2O_3 diffraction peaks are detected in the spectrum of sample

Table 2 The crystallite sizes of α-Al_2O_3 nanoparticles calcined at 1200 °C for 2 h

Sample	Peak height	X_s/nm
A	95.6	52.0
B	111.8	58.4
C	102.8	60.6
D	53.3	70.2

D. Calcination at 1200 °C for 2 h entirely converts sample C into α-Al_2O_3, whereas significant amount of θ- and δ-Al_2O_3 co-exist with α-Al_2O_3 in sample D. The XRD results for sample B are similar to those for sample C.

These results suggest that sample A has the lowest transformation temperature to α-Al_2O_3 and sample D has the highest. Sample A coverts into α-Al_2O_3 only through γ-Al_2O_3, without formation of other crystalline forms, as the calcination temperature is increased. But other crystalline forms are detected during the transformation to α-Al_2O_3 for the other three samples. Formation of α-Al_2O_3 *via* γ-Al_2O_3 is relatively easier than *via* θ-Al_2O_3 because the former transformation requires less energy.[16] This is why sample A has the lowest conversion temperature into α-Al_2O_3. The difference in calcination behaviour for these four samples may result from the different particle sizes. Nanoparticles usually show higher sintering activity and lower sintering temperature compared with their larger counterparts, and amorphous powders have relatively low recrystallisation temperatures.[24] Sample A has the smallest particle size, thus it shows the lowest conversion temperature to α-Al_2O_3. Accordingly, sample D has the highest conversion temperature due to its large particle size. It should be pointed out that sample C displays a larger apparent particle size than sample D, but shows a lower conversion temperature to α-Al_2O_3. This can be attributed to the fact that the hollow spherical particles in sample C are composed of small particles (Fig. 4), as determined by the mechanism of precipitation.

The (116) diffraction peak at $2\theta = 57.55°$ was chosen for the calculation of crystallite size using Scherrer's equation and the results are listed in Table 2. Similar results are obtained when using other diffraction peaks for the calculation. It is seen that samples A–C contain similar amounts of α-form crystallites, whereas sample D has less, as shown by the peak heights. However, sample A has smallest crystallite size, while sample D has the largest. It is expected that sample D would show even larger α-form crystallite sizes if it had the same crystallinity as the other samples. This result is consistent with the particle sizes and calcination behaviour of the nanopaticles.

4 Conclusions

Cyclohexane, Triton X-114 and 1.0 M $AlCl_3$ (aq) form a new ternary microemulsion system with a relatively high aqueous phase content and medium viscosity at 38 °C, and is particularly suitable for the preparation of Al_2O_3 nanoparticles.

Nano-sized Al_2O_3 particles were successfully synthesised in the microemulsions with a fixed oil-to-surfactant ratio of 70 : 30, but with various aqueous phase contents. The apparent dimension of the as-prepared nanoparticles is about 8 nm, which increases to some 15 nm after calcination under apropriate conditions. On the other hand, the as-prepared particles synthesised in the corresponding emulsion have a hollow spherical morphology constructed from nanoparticles, while direct precipitation from aqueous solution leads to much larger particles (*ca.* 250 nm).

The calcination behaviour of the resulting nanoparticles shows strong dependence on the synthetic conditions and, hence, the particle size. The nanoparticles synthesised in the bicontinuous microemulsion (sample A) are entirely converted into pure α-Al_2O_3 by calcination at 1100 °C for 2 h or 1000 °C for 12 h, whereas for the directly precipitated particles (sample D), α-Al_2O_3 can only be detected after treatment at 1200 °C, along with significant amounts of other crystal forms.

References

1 B. K. Paul and S. P. Moulik, *Curr. Sci.*, 2001, **80**, 990.
2 B. K. Paul and S. P. Moulik, *J. Dispersion Sci. Technol.*, 1997, **18**, 301.
3 J. Sjoblom, R. Lindberg and S. E. Friberg, *Adv. Colloid Interface Sci.*, 1996, **65**, 125.
4 F. J. Arriagada and K. Osseo-Asare, *Colloids Surf., A*, 1999, **154**, 311.
5 J. Wang, L. S. Ee, S. C. Ng, C. H. Chew and L. M. Gan, *Mater. Lett.*, 1997, **30**, 119.
6 G. L. Li and G. H. Wang, *Nanostruct. Mater.*, 1999, **11**, 663.
7 J. Fang, J. Wang, S. C. Ng, L. M. Gan, C. H. Quek and C. H. Chew, *Mater. Lett.*, 1998, **36**, 179.
8 L. S. Ee, J. Wang, S. C. Ng and L. M. Gan, *Mater. Res. Bull.*, 1998, **33**, 1045.
9 G. K. Lim, J. Wang, S. C. Ng, C. H. Chew and L. M. Gan, *Biomaterials*, 1997, **18**, 1433.
10 P. Tartaj and L. C. De Jonghe, *J. Mater. Chem.*, 2000, **10**, 2786.
11 H. Herrig and R. Hempelmann, *Mater. Lett.*, 1996, **27**, 287.
12 I. Balint, Zh. You and K. Aika, *Phys. Chem. Chem. Phys.*, 2002, **4**, 2501.
13 P. Tartaj and J. Tartaj, *Chem. Mater.*, 2002, **14**, 536.
14 K. T. Hwang, H. S. Lee, S. H. Lee, K. C. Chung, S. S. Park and J. H. Lee, *J. Eur. Ceram. Soc.*, 2001, **21**, 375.
15 R. N. Das, A. Bandyopadhyay and S. Bose, *J. Am. Ceram. Soc.*, 2001, **84**, 2421.
16 N. Bahlawane and T. Watanabe, *J. Am. Ceram. Soc.*, 2000, **83**, 2324.
17 J. Y. Choi and D. K. Kim, *J. Sol-Gel Sci. Technol.*, 1999, **15**, 231.
18 L. Laby, L. C. Klein, A. Turniansky and D. Avnir, *J. Sol-Gel Sci. Technol.*, 1997, **10**, 177.
19 R. H. G. A. Kiminami, M. R. Morelli, D. C. Folz and D. E. Clark, *J. Am. Ceram. Soc. Bull.*, 2000, **79**, 63.
20 P. M. Kumar, C. Balasubramanian, N. D. Sali, S. V. Bhoraskar, V. K. Rohatgi and S. Badrinarayanan, *J. Mater. Sci. Eng., B*, 1999, **63**, 215.
21 M. Lade, H. Mays, J. Schmidt, R. Willumeit and R. Schomäcker, *Colloids Surf., A*, 2000, **163**, 3.
22 H. Wennerstrom, O. Soderman, U. Olsson and B. Lindman, *Colloids Surf., A*, 1997, **123–124**, 13.
23 File no. 83-2384, PCPDFWIN version 2.1, JCPDS-International Centre for Diffraction Data, Newtown Square, PA, USA, 2000.
24 R. Thammler and R. Oberacker, *An Introduction to Powder Metallurgy*, The Institute of Materials, London, 1993, ch. 2, pp. 52–59.